Radar Autofocus Using Sparse Blind Deconvolution

Mansour, H.; Kamilov, U.S.; Liu, D.; Boufounos, P.T.

TR2018-003   April 2018

Abstract

The radar autofocus problem arises in situations where radar measurements are acquired of a scene using antennas that suffer from position ambiguity. Current techniques model the antenna ambiguity as a global phase error affecting the received radar measurement at every antenna. However, the phase error signal model is only valid in the far field regime where the position error can be approximated by a one dimensional shift in the down-range direction. We propose in this paper an alternate formulation where the antenna position error is modeled using a two-dimensional shift operator in the imagedomain. The radar autofocus problem then becomes a multichannel two-dimensional blind deconvolution problem where the static radar image is convolved with a two dimensional shift kernel for each antenna measurement. We develop an alternating minimization framework that leverages the sparsity and piece-wise smoothness of the radar scene, as well as the one-sparse property of the two dimensional shift kernels.

IEEE International Conference on Acoustics, Speech, and Signal Processing (ICASSP)

RADAR AUTOFOCUS USING SPARSE BLIND DECONVOLUTION

Hassan Mansour, Dehong Liu, Petros T. Boufounos

Mitsubishi Electric Research Laboratories,
201 Broadway, Cambridge, MA 02139, USA
{mansour,liudh,petrosb}@merl.com

*Ulugbek S. Kamilov**

Washington University in St. Louis,
St. Louis, MO 63130, USA
kamilov@wustl.edu

ABSTRACT

The radar autofocus problem arises in situations where radar measurements are acquired of a scene using antennas that suffer from position ambiguity. Current techniques model the antenna ambiguity as a global phase error affecting the received radar measurement at every antenna. However, the phase error signal model is only valid in the far field regime where the position error can be approximated by a one dimensional shift in the down-range direction. We propose in this paper an alternate formulation where the antenna position error is modeled using a two-dimensional shift operator in the image-domain. The radar autofocus problem then becomes a multichannel two-dimensional blind deconvolution problem where the static radar image is convolved with a two dimensional shift kernel for each antenna measurement. We develop an alternating minimization framework that leverages the sparsity and piece-wise smoothness of the radar scene, as well as the one-sparse property of the two dimensional shift kernels.

Index Terms— Radar autofocus, blind deconvolution, sparse image reconstruction, fused Lasso, block-coordinate descent

1. INTRODUCTION

High resolution radar imaging is a requirement in a variety of remote sensing applications including imaging with synthetic arrays and through-the-wall radar imaging (TWI). Whereas the down-range resolution is mostly controlled by the bandwidth of the transmitted pulse, the cross-range (azimuth) resolution depends on the aperture of the radar array. Generating a large physical aperture is practically achieved by deploying a number of distributed antennas or arrays, each having a relatively small aperture. A distributed setup allows for flexibility of platform placement, reduces the operational and maintenance costs, and adds robustness to sensor failures. Leveraging prior knowledge of the scene, such as sparsity, the precise knowledge of the antenna positions and a full synchronization of received signals has been shown to significantly improve the radar imaging resolution [1–4].

A fundamental challenge that arises in distributed array imaging comes from uncertainty in the exact positions of the antennas. While advanced positioning and navigation systems, such as the global navigation satellite system (GPS/GNSS) and the inertial navigation system (INS) provide somewhat accurate location information, the remainsing uncertainty in the true antenna positions can span multiple wavelengths. As a result, the received signal contains a gain and phase ambiguity when the inexact antenna positions are used as reference. Consequently, applying standard reconstruction techniques
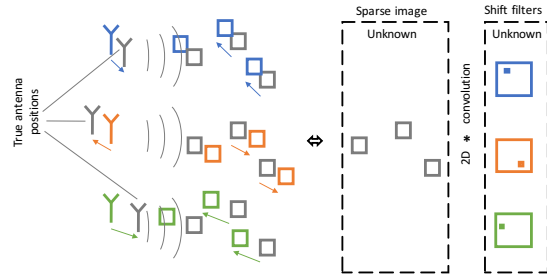
Fig. 1: Position ambiguity of the radar antennas induces an image-domain convolution model.

without accounting for the position perturbation produces out-of-focus radar images.

There have been a multitude of solutions that addressed the radar autofocus problem, particularly in the collocated antenna setting, by developing tools that compensate for the antenna position errors [6–11]. In some cases, the underlying structure of the radar image, such as its sparsity, is utilized to limit the solution space and produce higher quality reconstructions [12–18]. Fundamental to the autofocus problem is the task of resolving the gain and phase errors in the measured signal, which manifests as a blind deconvolution problem in the measurement domain. A rich body of literature has emerged recently for studying the identifiability and recovery guarantees of blind deconvolution algorithms [19–27]. Contrary to existing techniques that model the gain and phase ambiguity as a convolution in the measurement domain, we model every measured signal as an observation through the erroneous radar operator of a convolution between the static scene and a two-dimensional shift kernel.

We are interested in the problem of recovering an image of a stationary scene composed of sparse targets, and represented in vector form as $\mathbf{x} \in \mathbb{C}^N$. The image is to be recovered by processing F−dimensional frequency-domain measurements $\{\tilde{\mathbf{y}}_m\}_{m=1}^M$ from M distributed antennas that suffer from position ambiguity. We develop an image reconstruction framework wherein a perturbation in the antenna positions results in a measured signal that corresponds to an image-domain convolution model as illustrated in Figure 1. More precisely, if we denote the radar propagation matrix at the *correct* antenna positions by $\widetilde{\mathbf{A}}_m$, and denote by $\mathbf{A}_m$ the corresponding matrix at the *incorrect* positions, then we have $\tilde{\mathbf{y}}_m = \widetilde{\mathbf{A}}_m \mathbf{x} \neq \mathbf{A}_m \mathbf{x}$. Unfortunately, we are only provided the measurements $\tilde{\mathbf{y}}_m$ and the matrices $\mathbf{A}_m$. The position ambiguity of radar antennas can be modeled as a time-domain convolution with the measurements, or equivalently, as a gain and phase ambiguity in the frequency-domain of the radar signal, that is,

$$\tilde{\mathbf{y}}_m = \mathbf{D}_{\hat{\mathbf{g}}_m} \mathbf{A}_m \mathbf{x} + \mathbf{n}_m, \tag{1}$$

where $\mathbf{D}_{\hat{\mathbf{g}}_m}$ is a diagonal matrix with the phase correction vector $\hat{\mathbf{g}}_m \in \mathbb{C}^F$ on its diagonal entries, and $\mathbf{n}_m$ is a measurement noise vector. The system in (1) is ill-posed in general since for any M measurements, we are left with MF equations and $MF + N$ unknowns. Alternatively, we propose in this paper to represent the gain and phase ambiguity as an image-domain convolution where a two-dimensional spatial shift kernel $\mathbf{h}_m$ is applied to the radar image $\mathbf{x}$, i.e.,

$$\tilde{\mathbf{y}}_m = \mathbf{A}_m \left(\mathbf{x} * \mathbf{h}_m \right) + \mathbf{n}_m. \tag{2}$$

Under the new model, the shift kernels are one-sparse vectors with unknown support locations, thereby reducing the unknown degrees of freedom to $M \log(F) + N$.

We describe in Section 2 the radar signal model and prove that the image-domain convolution model is exact when the transmitting and receiving antennas are affected by the same position error. We then propose in Section 3 a block-coordinate descent algorithm that can efficiently solve the sparse blind deconvolution problem in the image domain. Finally, we present numerical simulations in Section 4 that validate our claims and demonstrate the effectiveness of our approach for solving the high resolution radar autofocus problem.

2. PROBLEM FORMULATION

2.1. Signal model

Consider a two-dimensional radar imaging scenario in which M distributed antennas are used to detect K targets. The targets are located within a spatial region of interest that is discretized on a grid $\Omega \subset \mathbb{R}^2, |\Omega| = N$, and $N = N_x \times N_y$ with N_x and N_y specifying the number of grid points in the horizontal and vertical directions. Denote by $l \in \Omega$ the spatial position of a grid-point in Ω.

Let $\Gamma \subset \mathbb{R}^2, |\Gamma| = M$ be the set of all the spatial locations of the M antennas. Without loss of generality, we shall assume that a subset of the antennas act as transmitter/receivers while the remaining antennas are only receivers. A transmitting antenna at position $r \in \Gamma$ emits a time-domain pulse $p(t)$ with frequency spectrum $P(\omega)$, where $\omega = 2\pi f$ is the angular frequency and $f \in \mathcal{B}$ is the ordinary frequency in the signal bandwidth $\mathcal{B}, |\mathcal{B}| = F$.

Denote by $\mathbf{y}_m := \mathbf{y}(r_m, r'_m)$ and by $\mathbf{A}_m := \mathbf{A}(r_m, r'_m)$ the corresponding measurement vector and imaging operator of antenna pair (r_m, r'_m) indexed by m. Let $\tilde{r}_m = r_m + e_m$ and $\tilde{r}'_m = r'_m + e'_m$ be the perturbed transmitter and receiver positions, respectively, where e_m and e'_m denote the positioning errors. The received antenna measurement $\tilde{\mathbf{y}}_m := \mathbf{y}(\tilde{r}_m, \tilde{r}'_m)$ observes the scene reflectivity $\mathbf{x}$ through the perturbed imaging operator $\widetilde{\mathbf{A}}_m := \mathbf{A}(\tilde{r}_m, \tilde{r}'_m)$, i.e.,

$$\tilde{\mathbf{y}}_m = \widetilde{\mathbf{A}}_m \mathbf{x} + \mathbf{n}_m. \tag{3}$$

Since the operator $\widetilde{\mathbf{A}}_m$ is unknown, we need to define the received measurements $\tilde{\mathbf{y}}_m$ as a function of $\mathbf{A}_m$ and $\mathbf{x}$.

2.2. Convolution in the measurement-domain

Standard approaches for radar autofocus utilize a gain and phase correction in the frequency measurement to describe $\tilde{\mathbf{y}}_m$ in terms of $\mathbf{A}_m$ and $\mathbf{x}$. More precisely, let $\hat{\mathbf{g}}_m \in \mathbb{C}^F$ be a complex valued vector corresponding to the Fourier transform of a time-domain kernel $\mathbf{g}_m \in \mathbb{R}^M$. The received measurement is expressed as in (1). Therefore, given M measurements $\tilde{\mathbf{y}}_m, m \in \{1 \dots M\}$, the radar autofocus problem is regarded as a bilinear inverse problem in both

the reflectivity image $\mathbf{x}$ and the phase correction vectors $\hat{\mathbf{g}}_m$ for all m.

Notice that the system in (1) has F equations with $F + N$ unknowns, which makes it severely ill-posed. Even in the case where $\mathbf{x}$ is sparse, the problem remains ill-posed since a general phase correction vector $\hat{\mathbf{g}}_m$ continues to have F degrees of freedom. In order to make the problem tractable, the kernels $\mathbf{g}_m = \mathbf{F}_1^{\mathsf{H}} \hat{\mathbf{g}}_m$ are often assumed to be shift kernels, which reduces its degrees of freedom to a singe phase angle. However, the approximation that $\mathbf{g}_m$ is a shift operator is only valid in the far field regime and where the position error can be approximated by a one dimensional shift in the down-range direction of the virtual antenna array.

2.3. Convolution in the image-domain

We propose here an alternate model to the convolution with a shift kernel in the measurement-domain by switching the convolution to the image-domain. Let $\mathbf{h}_m \in \mathbb{R}^{N_h^2}, N_h \leq \min\{N_x, N_y\}$ be a vectorized two-dimensional shift kernel of size $N_h \times N_h$. Under the new model, the received signal of the antenna pair indexed by m is written as in (2).

Proposition 1 shows that when the transmitting and receiving antennas are affected by the same position ambiguity, the convolution kernel $\mathbf{h}_m$ is strictly a spatial shift kernel with a single nonzero entry equal to one. This situation is prevalent in radar systems where the transmitting and receiving antennas are collocated. The system in (2) may still be underdetermined with F equations and $N_h^2 + N$ unknowns. However, given enough measurements, it should be possible to recover $\mathbf{x}$ and all shift kernels $\mathbf{h}_m$ by utilizing an appropriate regularization for each. We omit the proof due to space limitations but will include it in a longer version of this work.

Proposition 1. *Let $\tilde{\mathbf{y}}_m := \widetilde{\mathbf{A}}_m \mathbf{x}$, where $\mathbf{x}$ is a radar image defined over a spatial domain Ω. Denote by e_m and e'_m the position ambiguities for the transmitter and receiver antenna pair respectively indexed by m.*

If $e'_m = e_m$ and $\mathbf{x}$ is zero valued within a boundary of width e_m inside Ω, then there exists a spatially shifted image $\tilde{x}(l) = \delta(l + e_m) * x(l), \forall l \in \Omega$ such that $\tilde{\mathbf{y}}_m = \mathbf{A}_m \tilde{\mathbf{x}}$, where $\delta(l + e_m)$ is the two dimensional shift kernel.

Otherwise, if $e'_m = e_m + d_m$ with $\|d_m\|_2 \leq \Delta$, then the approximation $\tilde{\mathbf{y}}_m \approx \mathbf{A}_m \tilde{\mathbf{x}}$ incurs a phase error bounded by $e^{\pm i \omega \Delta / c}$ for each frequency ω.

3. PROPOSED APPROACH

Consider the image-domain convolution model expressed in the spatial Fourier domain below

$$\begin{aligned} \tilde{\mathbf{y}}_m &= \mathbf{A}_m \left(\mathbf{x} * \mathbf{h}_m \right) + \mathbf{n}_m \\ &= \mathbf{A}_m \mathbf{F}_2^{\mathsf{H}} \mathbf{D}_{\hat{\mathbf{h}}_m} \hat{\mathbf{x}} + \mathbf{n}_m, \end{aligned} \tag{4}$$

where $\mathbf{F}_2$ is the two dimensional Fourier transform operator applied to the vectorization of a matrix, $\hat{\mathbf{h}}_m = \mathbf{F}_2 \mathbf{h}_m$ and $\hat{\mathbf{x}} = \mathbf{F}_2 \mathbf{x}$ denote the two-dimensional Fourier transforms of $\mathbf{h}_m$ and $\mathbf{x}$, respectively, and $\mathbf{D}_{\hat{\mathbf{h}}_m}$ is the diagonal matrix with $\hat{\mathbf{h}}_m$ on the diagonal. We propose in this paper a block coordinate descent approach for computing the radar reflectivity image $\mathbf{x}$ and the spatial convolution filters $\mathbf{h}_m$ from noisy measurements $\tilde{\mathbf{y}}_m$.

We first incorporate into the model in (4) the prior information that the image $\mathbf{x}$ is sparse and piecewise continuous and that the kernels $\mathbf{h}_m$ are two dimensional shift operators. Therefore, we added

a *fused Lasso* [28] regularizer $\boldsymbol{R_x}(\cdot)$ for $\mathbf{x}$ and an ℓ_1 norm regularizer $\boldsymbol{R_h}(\cdot)$ to $\mathbf{h}_m$. The overall optimization problem is described as follows

$$\min_{\substack{\mathbf{x}\,\in\,\mathbb{C}^N, \\ \mathbf{h}_m\,\in\,\mathbb{R}_+^{N_h^2}}} \quad \sum_{m=1}^{M} \tfrac{1}{2}\|\tilde{\mathbf{y}}_m - \mathbf{A}_m\mathbf{F}_2^{\mathsf{H}}\mathbf{D}_{\hat{\mathbf{h}}_m}\hat{\mathbf{x}}\|_2^2$$
$$+\, \mu\boldsymbol{R_h}(\mathbf{h}_m) + \lambda\boldsymbol{R_x}(\mathbf{x}) \tag{5}$$

$$\text{subject to} \quad \mathbf{1}^T\mathbf{h}_m = 1, \forall\, m \in \{1\dots M\},$$

where $\mathbf{1}$ is the all one vector, and as before, $\hat{\mathbf{h}}_m = \mathbf{F}_2\mathbf{h}_m$ and $\hat{\mathbf{x}} = \mathbf{F}_2\mathbf{x}$. The parameters μ and λ are regularization parameters controlling the tradeoff between the signal priors and the data mismatch cost.

The *fused Lasso* regularizer $\boldsymbol{R_x}(\mathbf{x})$ combines the ℓ_1 norm and the total variation (TV) norm of a signal:

$$\boldsymbol{R_x}(\mathbf{x}) = \|\mathbf{x}\|_1 + \gamma\|\mathbf{x}\|_{TV}, \tag{6}$$

where the total variation norm is defined by

$$\|\mathbf{x}\|_{TV} := \|\mathbf{s}\|_{2,1} = \sum_{j=1}^{N}\sqrt{\mathbf{s}^2(j) + \mathbf{s}^2(N+j)}. \tag{7}$$

the sum of the ℓ_2 norms of groups of elements in the gradient vector $\mathbf{s} = \mathbf{E}\mathbf{x}$, where $\mathbf{E} : \mathbb{C}^N \to \mathbb{C}^{2N}$ is the two dimensional finite difference operator, such that, the first N entries of $\mathbf{s}$ contain the horizontal gradient coefficients, and the second N entries contain the vertical gradient coefficients. On the other hand, the property of a shift kernel requires that every $\mathbf{h}_m$ is one sparse with a nonzero entry equal to one. Since $\mathbf{h}_m$ is nonnegative with the sum of its entries equal to one, the only regularization required is the ℓ_1 norm penalty:

$$\boldsymbol{R_h}(\mathbf{h}_m) = \sum_{m=1}^{M}\|\mathbf{h}_m\|_1. \tag{8}$$

Algorithm 1 Block coordinate descent for solving (5)

    input: measurements $\{\tilde{\mathbf{y}}_m\}_{m=1}^{M}$, initial guess $\mathbf{x}^0, \mathbf{h}^0$, maximum subroutine iterations T, and regularization parameters λ, μ.
    set: $j \leftarrow 1; \tilde{\mathbf{h}}_m^0, \mathbf{h}_m^0 \leftarrow \mathbf{h}^0$ for all m
1: **repeat**
2:     $\mathcal{A}_{\mathbf{x}}^m \leftarrow \mathcal{A}_{\mathbf{x}}^m(\mathbf{h}_m^{j-1})$ for all m
3:     $\mathbf{x}^j \leftarrow \texttt{fista}(\{\mathcal{A}_{\mathbf{x}}^m\}_{m=1}^{M}, \lambda\boldsymbol{R_x}, \{\tilde{\mathbf{y}}_m\}_{m=1}^{M}, \mathbf{x}^{j-1}, T)$
4:     **for** $m \leftarrow 1$ to M **do**
5:         $\mathcal{A}_{\mathbf{h}}^m \leftarrow \mathcal{A}_{\mathbf{h}}^m(\mathbf{x}^j)$
6:         $\tilde{\mathbf{h}}_m^j \leftarrow \texttt{fista}(\mathcal{A}_{\mathbf{h}}^m, \mu\boldsymbol{R_h}, \tilde{\mathbf{y}}_m, \tilde{\mathbf{h}}_m^{j-1}, T)$
7:         $\mathbf{h}_m^j \leftarrow \boldsymbol{P}(\tilde{\mathbf{h}}_m^j)$
8:     $j \leftarrow j + 1$
9: **until** stopping criterion
    return: estimate of the radar image $\mathbf{x}^j$.

Clearly, problem (5) is nonconvex and our aim is to find a stationary point to the problem. Therefore, we present in Algorithm 1 a block coordinate descent approach that alternates between descent steps for each of $\mathbf{x}$ and $\mathbf{h}_m$, for all m. The shift kernels $\mathbf{h}_m$ are all initialized to the no-shift kernel $\mathbf{h}^0$, an $N_h \times N_h$ zero-valued matrix with the central entry set equal to one. For each descent step, we apply a small number of iterations of the fast iterative shrink-

age/thresholding algorithm (FISTA) [29] adapted to the appropriate regularizers of $\mathbf{x}$ or $\mathbf{h}_m$. Moreover, every descent step of $\mathbf{h}_m$, produces an estimate $\tilde{\mathbf{h}}_m$ which does not necessarily satisfy the shift kernel properties, since we only run a small number of FISTA iterations. Therefore, we use a projector $\boldsymbol{P}(\tilde{\mathbf{h}}_m)$ onto the space of shift kernels which sparsifies $\tilde{\mathbf{h}}_m$ by setting its largest entry that is closest to the center to one and setting the remaining entries to zero.

Algorithm 2 `fista` subroutine for updating $\mathbf{h}_m$

    input: $\mathcal{A}_{\mathbf{h}}^m, \mu\boldsymbol{R_h}, \tilde{\mathbf{y}}_m, \tilde{\mathbf{h}}_m^{j-1}, T$.
    set: $q_0 = 1, \mathbf{u}^0 = \mathbf{s}^0 = \tilde{\mathbf{h}}_m^{j-1}$
1: $\alpha \leftarrow$ inverse of maximum eigenvalue of $\mathcal{A}_{\mathbf{h}}^{m\mathsf{H}}\mathcal{A}_{\mathbf{h}}^m$
2: **for** $t \leftarrow 1$ to T **do**
3:     $\mathbf{z}^t \leftarrow \mathbf{s}^{t-1} + \alpha\mathcal{A}_{\mathbf{h}}^{m\mathsf{H}}(\tilde{\mathbf{y}}_m - \mathcal{A}_{\mathbf{h}}^m\mathbf{s}^{t-1})$
4:     $\mathbf{u}^t \leftarrow \mathcal{T}_+(\mathbf{z}^t; \alpha\mu)$
5:     $\mathbf{u}^t \leftarrow \frac{1}{\mathbf{1}^T\mathbf{u}^t}\mathbf{u}^t$
6:     $q_t \leftarrow \frac{1+\sqrt{1+4q_{t-1}^2}}{2}$
7:     $\mathbf{s}^t \leftarrow \mathbf{u}^t + \frac{q_{t-1}-1}{q_t}(\mathbf{u}^t - \mathbf{u}^{t-1})$
    return: $\mathbf{s}^T$.

Algorithm 3 `fista` subroutine for updating $\mathbf{x}$

    input: $\{\mathcal{A}_{\mathbf{x}}^m\}_{m=1}^{M}, \lambda\boldsymbol{R_x}, \{\tilde{\mathbf{y}}_m\}_{m=1}^{M}, \mathbf{x}^{j-1}, T$.
    set: $q_0 = 1, \mathbf{u}^0 = \mathbf{s}^0 = \mathbf{x}^{j-1}$
1: $\alpha \leftarrow$ inverse of maximum eigenvalue of $\sum_{m=1}^{M}\mathcal{A}_{\mathbf{x}}^{m\mathsf{H}}\mathcal{A}_{\mathbf{x}}^m$
2: **for** $t \leftarrow 1$ to T **do**
3:     $\mathbf{z}^t \leftarrow \mathbf{s}^{t-1} + \alpha\sum_{m=1}^{M}\mathcal{A}_{\mathbf{x}}^{m\mathsf{H}}(\tilde{\mathbf{y}}_m - \mathcal{A}_{\mathbf{x}}^m\mathbf{s}^{t-1})$
4:     $\mathbf{v}^t \leftarrow \mathcal{T}(\mathbf{z}^t; \alpha\lambda)$
5:     $\mathbf{u}^t \leftarrow \arg\min_{\mathbf{u}\in\mathbb{C}^N}\left\{\tfrac{1}{2}\|\mathbf{u} - \mathbf{v}^t\|_2^2 + \alpha\lambda\gamma\|\mathbf{u}\|_{TV})\right\}$
6:     $q_t \leftarrow \frac{1+\sqrt{1+4q_{t-1}^2}}{2}$
7:     $\mathbf{s}^t \leftarrow \mathbf{u}^t + \frac{q_{t-1}-1}{q_t}(\mathbf{u}^t - \mathbf{u}^{t-1})$
    return: $\mathbf{s}^T$.

In general, FISTA can be used to solve convex optimization problems of the form

$$\min_{\mathbf{u}\in\mathcal{S}} \boldsymbol{D}(\mathbf{u}) + \lambda\boldsymbol{R}(\mathbf{u}), \tag{9}$$

where $\boldsymbol{D}(\mathbf{u})$ is a smooth data fidelity cost function and $\boldsymbol{R}$ is a regularizer which can be a non-smooth function. In the context of Algorithm 1, we define the subroutine $\texttt{fista}(\mathcal{A}^m, \boldsymbol{R}, \mathbf{y}_m, \mathbf{u}_{\text{init}}, T)$ as an algorithm that runs T iterations of the FISTA procedure with a data fidelity cost function $\boldsymbol{D}(\mathbf{u})$, regularizer $\boldsymbol{R}$, and initial guess $\mathbf{u}_{\text{init}}$. The data fidelity cost function is specified by (5) as

$$\boldsymbol{D}(\mathbf{u}) := \sum_{m=1}^{M}\frac{1}{2}\|\tilde{\mathbf{y}}_m - \mathcal{A}^m\mathbf{u}\|_2^2, \tag{10}$$

where $\mathbf{u}$ refers to either the image $\mathbf{x}$ or the sequence of convolution kernels $\mathbf{h}_m$. The forward operator with the respect to $\mathbf{x}$ given the estimates of the kernels $\mathbf{h}_m^t$ at iteration t is defined as

$$\mathcal{A}_{\mathbf{x}}^m(\mathbf{h}_m^t) := \mathbf{A}_m\mathbf{F}_2^{\mathsf{H}}\mathbf{D}_{\mathbf{F}_2\mathbf{h}_m^t}\mathbf{F}_2. \tag{11}$$

Similarly, the forward operator with respect to $\mathbf{h}_m$ given the estimate

of the image $\mathbf{x}^t$ at iteration t is defined as

$$\mathcal{A}_{\mathbf{h}}^m(\mathbf{x}^t) := \mathbf{A}_m \mathbf{F}_2^{\mathsf{H}} \mathbf{D}_{\mathbf{F}_2 \mathbf{x}^t} \mathbf{F}_2. \qquad (12)$$

Note that the expression for $\boldsymbol{D}$ in (10) is separable in $\mathbf{h}_m$ for every m. Therefore, the FISTA subroutines for updating $\mathbf{h}_m$ and $\mathbf{x}$ are described in Algorithm 2 and Algorithm 3, respectively. The function $\mathcal{T}\left(\mathbf{z}^t; \alpha\lambda\right)$ is the standard soft-thresholding operator defined as

$$\mathcal{T}\left(\mathbf{z}; \tau\right) = \begin{cases} \mathbf{z}(j) - \tau, & \text{if } \mathbf{z}(j) > \tau \\ \mathbf{z}(j) + \tau, & \text{if } \mathbf{z}(j) < -\tau \\ 0, & \text{otherwise.} \end{cases} \qquad (13)$$

The function $\mathcal{T}_+\left(\mathbf{z}; \tau\right)$ is the non-negative counterpart that excludes the second condition in (13). We handle the combined ℓ_1 norm and total variation regularizers of $\mathbf{x}$ by splitting the proximal operators into the two stages shown in steps 4 and 5 of Algorithm 3. In the first stage, the soft-thresholding operator $\mathcal{T}\left(\mathbf{z}^t; \alpha\lambda\right)$ is used to sparsify the signal $\mathbf{z}^t$. A second proximal operator is then applied in step 5 of the algorithm to enforce the total variation regularization. We implement this proximal operator using an alternating direction method of multipliers (ADMM) algorithm [30, 31].

4. PERFORMANCE EVALUATION

We evaluate the performance of our radar autofocus framework using the simulation setup shown in Figure 2. The figure illustrates a radar scene acquired by 32 distributed antennas divided into four arrays with average position error around 2λ and maximum error at 3.5λ, where λ is the wavelength of the center frequency of a differential Gaussian pulse centered at 6 GHz with a 9 GHz bandwidth. The true antenna positions are indicated by the $\times$'s whereas the erroneous assumed positions are indicated by the dots. The received signals are contaminated with white Gaussian noise at 30 dB peak signal to noise ratio (PSNR) after matched-filtering with the transmitted pulse. Figure 3(a) shows the ground truth recovery where the correct antenna positions are used. Contrast that with Figure 3(b) where the incorrect antenna positions are used in constructing the radar propagation matrix. The advantage of the image-domain convolution model becomes evident when we compare the recovery performance in Figures 3(c) and 3(d). While the measurement-domain convolution model can provide an approximation of the radar scene as observed in Figure 3(c), the image-domain convolution model produces an exact reconstruction of the scene in Figure 3(d) up to a global shift ambiguity.
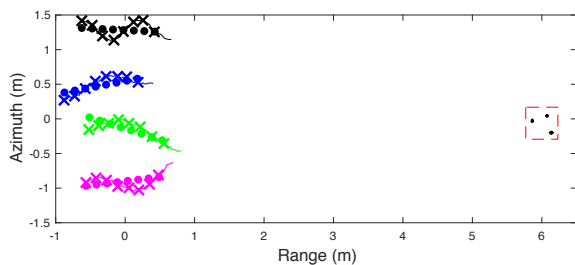

Fig. 2: A distributed radar acquisition system with position ambiguity. The round dots indicate the assumed but erroneous antenna positions, while the $\times$'s indicate the true positions.
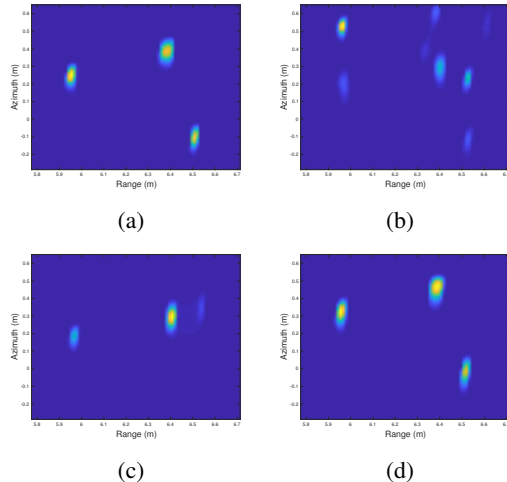

Fig. 3: (a)–(b) Sparse recovery of radar images without autofocusing obtained using (a) the correct antenna positions, and (b) the incorrect antenna positions. (c)–(d) Autofocus results using blind deconvolution according to (c) the time-domain convolution model; and (d) using the proposed sparse blind deconvolution and the image-domain convolution model.
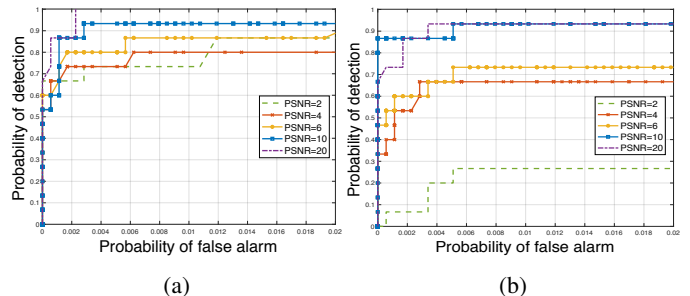

Fig. 4: ROC curves of the reconstructed images using (a) the proposed sparse blind deconvolution scheme, and (b) the iterative perturbation estimation scheme of [16].

Next, we compare the robustness of our proposed approach to the state of the art iterative perturbation estimation scheme of [16]. The method in [16] leverages the sparsity of the radar scene as well as the proximity between consecutive antenna positions in order to estimate the antenna perturbations and consequently improve the reconstructed image quality. To that end, we consider the radar scene shown in Figure 2 and contaminate the measurements with additive white Gaussian noise to the effect of producing PSNR levels equal to 2, 4, 6, 10, and 20 dB. Since the scheme in [16] relies on the antenna proximity to perform coherence analysis, we allow it to use additional measurements at antenna positions that interpolate the gaps between the $\times$'s for a total of 52 antenna positions per array. On the other hand, our proposed method uses only eight antenna positions per array. We compare the reconstruction performance in terms of the receiver operating characteristic (ROC) curves as shown in Figure 4. To generate the ROC curves, we simulate five different target positions as well as five different antenna perturbations and noise realizations. It can be seen from the figure that our proposed method is significantly more robust to measurement noise even at extremely high noise levels.

5. REFERENCES

[1] M. A. Herman and T. Strohmer, "High-resolution radar via compressed sensing," *IEEE Transactions on Signal Processing*, vol. 57, no. 6, pp. 2275–2284, June 2009.

[2] Y. Yu, A. P. Petropulu, and H. V. Poor, "Mimo radar using compressive sampling," *IEEE Journal of Selected Topics in Signal Processing*, vol. 4, no. 1, pp. 146–163, Feb 2010.

[3] C. R. Berger and J. M. F. Moura, "Noncoherent compressive sensing with application to distributed radar," in *2011 45th Annual Conference on Information Sciences and Systems*, March 2011, pp. 1–6.

[4] D. Liu, U. S. Kamilov, and P. T. Boufounos, "Sparsity-driven distributed array imaging," in *2015 IEEE 6th International Workshop on Computational Advances in Multi-Sensor Adaptive Processing (CAMSAP)*, Dec 2015, pp. 441–444.

[5] L. Wang, B. Yazıcı, and H. C. Yanik, "Antenna motion errors in bistatic sar imagery," *Inverse Problems*, vol. 31, no. 6, p. 065001, 2015. [Online]. Available: http://stacks.iop.org/0266-5611/31/i=6/a=065001

[6] D. E. Wahl, P. H. Eichel, D. C. Ghiglia, and C. V. Jakowatz, "Phase gradient autofocus-a robust tool for high resolution sar phase correction," *IEEE Transactions on Aerospace and Electronic Systems*, vol. 30, no. 3, pp. 827–835, Jul 1994.

[7] L. Xi, L. Guosui, and J. Ni, "Autofocusing of isar images based on entropy minimization," *IEEE Transactions on Aerospace and Electronic Systems*, vol. 35, no. 4, pp. 1240–1252, Oct 1999.

[8] W. Ye, T. S. Yeo, and Z. Bao, "Weighted least-squares estimation of phase errors for sar/isar autofocus," *IEEE Transactions on Geoscience and Remote Sensing*, vol. 37, no. 5, pp. 2487–2494, Sep 1999.

[9] H. J. Cho and D. C. Munson, "Overcoming polar-format issues in multichannel sar autofocus," in *2008 42nd Asilomar Conference on Signals, Systems and Computers*, Oct 2008, pp. 523–527.

[10] K. H. Liu and D. C. Munson, "Fourier-domain multichannel autofocus for synthetic aperture radar," *IEEE Transactions on Image Processing*, vol. 20, no. 12, pp. 3544–3552, Dec 2011.

[11] M. P. Nguyen and S. B. Ammar, "Second order motion compensation for squinted spotlight synthetic aperture radar," in *Conference Proceedings of 2013 Asia-Pacific Conference on Synthetic Aperture Radar (APSAR)*, Sept 2013, pp. 202–205.

[12] N. O. Onhon and M. Cetin, "A sparsity-driven approach for joint sar imaging and phase error correction," *IEEE Transactions on Image Processing*, vol. 21, no. 4, pp. 2075–2088, April 2012.

[13] X. Du, C. Duan, and W. Hu, "Sparse representation based autofocusing technique for isar images," *IEEE Transactions on Geoscience and Remote Sensing*, vol. 51, no. 3, pp. 1826–1835, March 2013.

[14] S. Kelly, M. Yaghoobi, and M. Davies, "Sparsity-based autofocus for undersampled synthetic aperture radar," *IEEE Transactions on Aerospace and Electronic Systems*, vol. 50, no. 2, pp. 972–986, April 2014.

[15] J. Yang, X. Huang, J. Thompson, T. Jin, and Z. Zhou, "Compressed sensing radar imaging with compensation of observation position error," *IEEE Transactions on Geoscience and Remote Sensing*, vol. 52, no. 8, pp. 4608–4620, Aug 2014.

[16] D. Liu, U. S. Kamilov, and P. T. Boufounos, "Coherent distributed array imaging under unknown position perturbations," in *4th International Workshop on Compressed Sensing Theory and its Applications to Radar, Sonar and Remote Sensing (CoSeRa)*, Sept 2016, pp. 105–109.

[17] L. Zhao, L. Wang, G. Bi, S. Li, L. Yang, and H. Zhang, "Structured sparsity-driven autofocus algorithm for high-resolution radar imagery," *Signal Processing*, vol. 125, pp. 376 – 388, 2016.

[18] M. J. Hasankhan, S. Samadi, and M. Çetin, "Sparse representation-based algorithm for joint sar image formation and autofocus," *Signal, Image and Video Processing*, vol. 11, no. 4, pp. 589–596, May 2017.

[19] A. Ahmed, B. Recht, and J. Romberg, "Blind deconvolution using convex programming," *IEEE Transactions on Information Theory*, vol. 60, no. 3, pp. 1711–1732, March 2014.

[20] A. Ahmed and L. Demanet, "Leveraging diversity and sparsity in blind deconvolution," *arXiv:1610.06098*, 2016.

[21] Ç. Bilen, G. Puy, R. Gribonval, and L. Daudet, "Convex optimization approaches for blind sensor calibration using sparsity," *IEEE Transactions on Signal Processing*, vol. 62, no. 18, pp. 4847–4856, Sept 2014.

[22] S. Ling and T. Strohmer, "Self-calibration and biconvex compressive sensing," *Inverse Problems*, vol. 31, no. 11, p. 115002, 2015. [Online]. Available: http://stacks.iop.org/0266-5611/31/i=11/a=115002

[23] ——, "Self-calibration and bilinear inverse problems via linear least squares," *arXiv:1611.04196*, 2016.

[24] L. Wang and Y. Chi, "Blind deconvolution from multiple sparse inputs," *IEEE Signal Processing Letters*, vol. 23, no. 10, pp. 1384–1388, Oct 2016.

[25] Y. Li, K. Lee, and Y. Bresler, "Optimal sample complexity for blind gain and phase calibration," *IEEE Transactions on Signal Processing*, vol. 64, no. 21, pp. 5549–5556, Nov 2016.

[26] ——, "Identifiability in bilinear inverse problems with applications to subspace or sparsity-constrained blind gain and phase calibration," *IEEE Transactions on Information Theory*, vol. 63, no. 2, pp. 822–842, Feb 2017.

[27] K. Lee, N. Tian, and J. Romberg, "Fast and guaranteed blind multichannel deconvolution under a bilinear system model," *arXiv:1610.06469*, 2016.

[28] R. Tibshirani, M. Saunders, S. Rosset, J. Zhu, and K. Knight, "Sparsity and smoothness via the fused lasso," *Journal of the Royal Statistical Society: Series B (Statistical Methodology)*, vol. 67, no. 1, pp. 91–108, 2005.

[29] A. Beck and M. Teboulle, "A fast iterative shrinkage-thresholding algorithm for linear inverse problems," *SIAM Journal on Imaging Sciences*, vol. 2, no. 1, pp. 183–202, 2009.

[30] J. Douglas and H. H. Rachford, "On the numerical solution of heat conduction problems in two and three space variables," *Transaction of the American Mathematical Society*, vol. 82, pp. 421–489, 1956.

[31] S. Boyd, N. Parikh, E. Chu, B. Peleato, and J. Eckstein, "Distributed optimization and statistical learning via the alternating direction method of multipliers," *Found. Trends Mach. Learn.*, vol. 3, no. 1, pp. 1–122, Jan. 2011.